Biochemical and Biophysical Research Communications **254,** 174–180 (1999)
Article ID bbrc.1998.9898, available online at http://www.idealibrary.com on IDEAL®

Secondary Structure of Sea Anemone Cytolysins in Soluble and Membrane Bound Form by Infrared Spectroscopy

Gianfranco Menestrina,*[,1] Veronique Cabiaux,† and Mayra Tejuca*[,‡]
**CNR-ITC, Centro di Fisica degli Stati Aggregati, Via Sommarive 18, I-38050 Povo, Trento, Italy; †Lab.Macromolecules aux Interfaces, Univ.Libre Bruxelles, Blvd. du Triomphe, 1050 Brussels Belgium; and ‡Departamento de Bioquimica, Facultad de Biologia, Universidad de la Habana, Calle 23 e/ I y J, La Habana, Cuba*

Received November 24, 1998

Attenuated total reflection (ATR) Fourier transform infrared spectroscopy (FTIR) was used to investigate the secondary structure of two pore-forming cytolysins from the sea anemone *Stichodactyla helianthus* and their interaction with lipid membranes. Frequency component analysis of the amide I' band indicated that these peptides are composed predominantly of beta structure, comprising 44–50% β-sheet, 18–20% β-turn, 12–15% α-helix, and 19–22% random coil. Upon interaction with lipid membranes a slight increase in the α-helical and β-sheet structures was observed with a concomitant decrease of the unordered structure. Polarisation experiments indicated that both toxins had some disordering effect on the lipid layers. The dichroic ratio of the α-helical component of the membrane-bound toxin was 3.0-3.3, indicating that this element was oriented with an angle of 38°–42° with respect to the normal to the plane of the crystal surface, thus resulting almost parallel to the mean direction of the lipid chains.

Sea anemones contain in their venom at least one, but usually a few, cytolysins belonging to a protein familiy collectively called actinoporins (1-3). These are polypeptides with a high pI, a molecular size around 20 kDa, and a high degree of homology, which are all inhibited by sphingomyelin. They probably share also the mechanism of toxicity, which appears to be that of opening pores in the membrane of foreign cells (4-6). Pore-forming toxins are widespread in nature. Several examples are known of animal, plant and bacterial origin (7, 8). Nevertheless, a clear picture of the structure and function of these proteins is still missing. Information on 3D structures are for the moment available only for a few bacterial toxins (9, 10), and are probably of limited value for predicting the structure of eukaryotic toxins. Indeed, sea anemone cytolysins are apparently not related to any other protein (11). High resolution structural data on actinoporins are still missing, and only general notions to this regard have been derived from indirect experiments. They may form pores by aggregation of several monomers, three to four, into the lipid phase (5, 6, 12, 13); adsorbtion may be preceded by a transition to a relaxed, molten globule-like, structural intermediate (14); insertion into the membrane involves more than one region of the molecule, at least the N-terminus (15) and a central hydrophobic region containing a cluster of 3 tryptophan residues (16).

Here we have used Fourier transform infrared spectroscopy, in the attenuated total reflection configuration (FTIR-ATR), to investigate the secondary structure of two such pore-forming cytolysins, sticholysin I and II, isolated from the sea anemone *Stichodactyla helianthus.* This technique, although providing only low resolution structural data, is indeed one of the few available to study the interaction of proteins with lipid membranes (17, 18). Our results are consistent with the notion that the formation of toxin channels is accompanied by a small conformational change of these proteins, leading to an increased amount of α-helical content and to a change in the β-sheet signal consistent with the formation of intramolecular (presumably monomer-monomer) bindings. The helix component is oriented perpendicularly to the plane of the membrane although not necessarily inserted in it.

MATERIALS AND METHODS

Toxins. Sticholysin I and II from *Stichodactyla helianthus,* (called St I and St II respectively), were purified by two consecutive

[1] Corresponding author. Fax: 39 461 810628. E-mail: menes@cefsa.itc.it.

0006-291X/99 $30.00

chromatographic steps (5). Briefly, total extracts from the sea anemone body were gel filtered on Sephadex G50, and the second eluting peak, which contained most of the hemolytic activity, was subjected to ion-exchange chromatography on a CM-52 cellulose column. Two peaks were thus separated, that eluting at the lower ionic strength was called St I and the other St II. Both proteins were sequenced. According to its primary structure (Swissprot P07845) St II corresponds to the cytolysin C III previously isolated by Blumenthal and Kem (19). St I instead has the same N-terminus sequence as the toxin called C I by Kem and Dunn (20).

Determination of the hemolytic activity. Hemolytic activity was determined on human erythrocytes (HRBC) by measuring the turbidity at 650 nm with a 96-well microplate reader (Molecular Devices UV-max) as described earlier (21).

Preparation of lipid vesicles. Large unilamellar lipid vesicles (LUV) were prepared by extruding a solution of multilamellar liposome in 10 mM Hepes-Cl, pH 8.0 (buffer A) subjected to 5 or 6 cycles of freezing and thawing (22). Thirty one passages were performed through two stacked polycarbonate filters with holes of 200 nm average diameter (purchased from Nucleopore), using the two-syringes extruder LiposoFast from Avestin Inc., Ottawa, Canada. The lipids used were egg phosphatidylcholine (PC) and sphingomyelin (SM), both purchased by Avanti Polar Lipids, more than 99% pure. They were mixed in a 1:1 molar ratio at a final concentration of 5 mg/ml.

Preparation of membrane bound toxin. Aliquots of PC:SM LUV, prepared as described above, were diluted to 0.45 mM in 2.2 ml of buffer A and incubated with 1.8 μM of one of the two sticholysins (final molar ratio lipid:toxin 250:1). After incubation at room temperature for ½ h, the LUVs were separated from the residual unbound toxin by precipitation in an ultracentrifuge (Optima TL 100 by Beckman). Samples were loaded in a swing-out rotor (TLS 55) and run at 49 krpm (≈180,000×g) for 3 h at 5°C. The supernatants were collected and tested for the presence of free toxin by measuring the hemolytic activity. The pellet, consisting of vesicles and bound toxin, was recollected in 100 μl of buffer A, and subjected to FTIR analysis. Controls in which the same amount of toxin was centrifuged in the absence of the vesicles indicated that, without lipid, the protein does not precipitate with this treatment.

Fourier-transform infrared spectroscopy. FTIR spectra were collected on a Bio-Rad FTS 185 spectrometer equipped with a DTGS detector with CsI window and KBr beamsplitter. The instrument was purged with CO_2-free dry air. The attenuated total reflection (ATR) configuration was used (18, 23, 24) with a 10-reflections Ge crystal (45° cut) housed in a liquid cell and placed in an ATR attachment by Specac. Typically 48 interferograms (64 in the case of the pure lipids) were collected, Fourier transformed and averaged. Absorption spectra in the region between 4000 and 1000 cm^{-1}, at a resolution of one data point every 0.25 cm^{-1}, were obtained using a clean crystal as the background. For the study of the toxins in soluble form, 40 μl of a 1 mg/ml protein solution, extensively dialysed against buffer A, were deposited and gently dried under nitrogen in a thin layer on one side of the crystal. This is a commonly adopted procedure (25, 26) which does not remove the hydration water that clearly appears in the region around 3500 cm^{-1} of the IR spectrum. For the lipid-bound toxin, 90 μl of the toxin-treated LUV pellet described above, were spread similarly. Spectra of the lipid alone were collected applying toxin-free LUV in the same way. After collecting spectra in a water saturated environment, the crystal was flushed with D_2O-saturated nitrogen for 30-40 min to allow deuteration of the fast-exchangeable amide hydrogen ions and new, deuterated, spectra were collected (17, 27).

ATR-FTIR spectra were processed using the Bio-Rad Win-Ir software package. First, the residual H_2O vapour bands were removed and a linear baseline between 1720 and 1500 cm^{-1} was subtracted. Then, the amide I' band, between 1700 and 1600 cm^{-1}, was deconvoluted and the number, position, amplitude and width of its Lorentzian components was determined. These were used as a starting point for a final refinement based on a least-squares fit of the original spectrum with the Levenberg-Marquardt method (23, 24). The relative content of structural elements was eventually estimated by dividing the areas of the individual components, assigned to a particular secondary structure in the standard way (23, 28), by the area of the whole amide I' band. The two small components around 1614 cm^{-1} and 1600 cm^{-1}, arising from the contribution of the side chains (29), were excluded from the sum. In the case of lipid-bound toxin, before analysis, the spectra were corrected by subtracting the contribution of the lipid alone (with a weight that eliminates the band at 1738 cm^{-1} pertaining to the stretching of the phospholipid carboxyl groups). This was necessary also in view of the fact that sphingomyelin, comprising the ceramide moiety, contributed a signal in the amide I region which was between 30 and 40% of the total. After removal of the lipid contribution, differential spectra were also obtained by subtracting the spectrum of the toxin in soluble form, with a weight that minimises the remaining integral in the amide I' region.

Quantitative analysis of the polarised ATR-IR spectra. In the case of lipids and lipid-bound toxins, the orientation of some structural elements was determined by polarisation experiments. A rotating wire-grid polariser from Specac was used and manually positioned with orientation either parallel (0°) or perpendicular (90°) to the plane of the internal reflections. The dichroic ratio was calculated as $R = A_{0°}/A_{90°}$, where $A_{0°}$ and $A_{90°}$ are the integrated absorbtion bands in the parallel and perpendicular configuration respectively. From the dichroic ratio a form factor, S, was calculated as (18, 30, 31):

$$S = \frac{E_x^2 - RE_y^2 + E_z^2}{\frac{1}{2}(3\cos^2\theta - 1)(E_x^2 - RE_y^2 - 2E_z^2)} \qquad \text{[Eq. 1]}$$

where θ is the angle between the long axis of the molecule under consideration and the transition moment of the investigated vibration; E_x, E_y and E_z are the components of the electric field of the evanescent wave in the three directions (the z axis being perpendicular to the plane of the crystal). The terms E_x^2, E_y^2 and E_z^2 were calculated according to Harrick expressions for thick films (30-32) using the appropriate incidence angle (45°) and refractive indexes (Ge crystal 4, deposited layer 1.43). The following order parameters were calculated: a) S_L, for the lipid chains, using either the symmetric or asymmetric CH_2 stretching (i.e. integrating the bands centred at 2850 and 1918 cm^{-1} respectively, with $\theta = 90°$) or the asymmetric CH_3 stretching (band at 2872 cm^{-1} with $\theta = 0°$); b) $S_{amide\ I'}$, for the whole amide I' band, integrating between 1600 and 1700 cm^{-1}, with $\theta = 0°$ (33, 34); c) S_α, for the α-helix, using the Lorentzian component at 1655 ± 2 cm^{-1} with $\theta = 30°$ (25, 31, 35).

From the order parameter the average tilt angle γ of the molecular axis with respect to the z axis (i.e. the perpendicular to the plane of the membrane) was calculated according to (31):

$$S = \tfrac{1}{2}(3\cos^2\gamma - 1) \qquad \text{[Eq. 2]}$$

Alternatively, the mean angle σ of the α-helix axis with respect to the direction of the lipid chains was recalculated from (31):

$$\frac{S_\alpha}{\frac{1}{2}(3\cos^2\gamma_L - 1)} = \tfrac{1}{2}(3\cos^2\sigma - 1) \qquad \text{[Eq. 3]}$$

where γ_L is the angle formed by the lipid chains with the z axis.

According to (33, 34), $A_{90°}$ was also used to calculate the lipid to toxin ratio (r) by the following algorithm:

$$r = L/T_b = \frac{(n_{res} - 1)}{9.6} \frac{1 - S_{amide\ I'}}{1 + S_L/2} \frac{\int_{2800}^{2980} A_{90°}(\nu_L)\, d\nu}{\int_{1600}^{1690} A_{90°}(\nu_{amide\ I'})\, d\nu} \quad [Eq.\ 4]$$

where L is the total concentration of lipid present, T_b is the concentration of bound toxin, n_{res} is the total number of residues in the toxin (176 for St I and 175 for St II), S_L and $S_{amide\ I'}$ have been defined above and the integrals refer to the corrected spectra. From r, it is possible to calculate the partition coefficient (K) of the protein from the water to the lipid phase as follows:

$$K = \frac{T_b}{(T_0 - T_b) \cdot L} = \frac{1}{T_0 \cdot r - L} \quad [Eq.\ 5]$$

where T_0 is the total concentration of toxin applied.

RESULTS AND DISCUSSION

Secondary structure of sticholysins by FTIR spectroscopy. The secondary structure of St I and II was estimated by analysing the amide I' band, as exemplified in Fig. 1 for the case of St II. Spectra were first deconvoluted to find out the number and location of the adsorption bands composing the whole amide region (Fig. 1B). Thereafter the original spectra were fitted to the sum of single Lorentzian bands (Fig. 1A) and these were attributed to four secondary structures (β-turn, α-helix, random coil and β-sheet), according to the accepted interpretation (17, 24, 28). Average compositions are reported in Table 1. As it could be expected from the fact that the primary sequences of St I and II are very similar (93.1% identity plus 1.7% similarity), it appears that both proteins had almost the same conformation. In particular, they are largely composed of β-structure, comprising 44-50% β-sheet plus 18-20% β-turn, and only 12-15% α-helix and 19-22% random coil. This finding clearly justifies the family name of actinoporins that was given to these group of cytolysins because of a very limited homology to a bacterial porin (19). The composition found here is not substantially different from that determined earlier for equinatoxin II (another actinoporin of *Actinia equina*) by circular dichroism (36) although slightly more helical structure was determined in that case. Interestingly, on the basis of a comparison of their primary sequences, this protein family shares the presence of a conserved amphipathic alpha-helix of at least 23 residues at the N-terminus (36). By itself, this helix would amount to approximately 13% of the protein, thus leaving little space for the presence of other helical elements in these molecules.

To get some insight into the conformational changes that might accompany the insertion of these toxins into the membrane, and eventually the formation of pores, we evaluated their secondary structure once bound to LUV. In a differential spectrum, obtained by subtracting the spectrum of the soluble form from that of the lipid bound form, small, but clear, changes were observed (Fig. 2B). An excess of absorbance at 1656 cm^{-1} (consistent with an increase in α-helical structure), a negative region centred around 1640 cm^{-1} (suggesting a decrease in the unordered structure), and another excess of absorbance at 1624 cm^{-1} (consistent with an increase in the β^2 region). Also in this case, the pattern was substantially similar for St II and St I, although with St II the α-helical increase was slightly higher, and the β^2 increase slightly lower. Application of the curve fitting procedure used for the free toxins to the membrane bound spectra, essentially confirmed these observations (Table 1). Interestingly, the raising β^2 band at 1624 cm^{-1} is indicative of a peculiar hydrogen

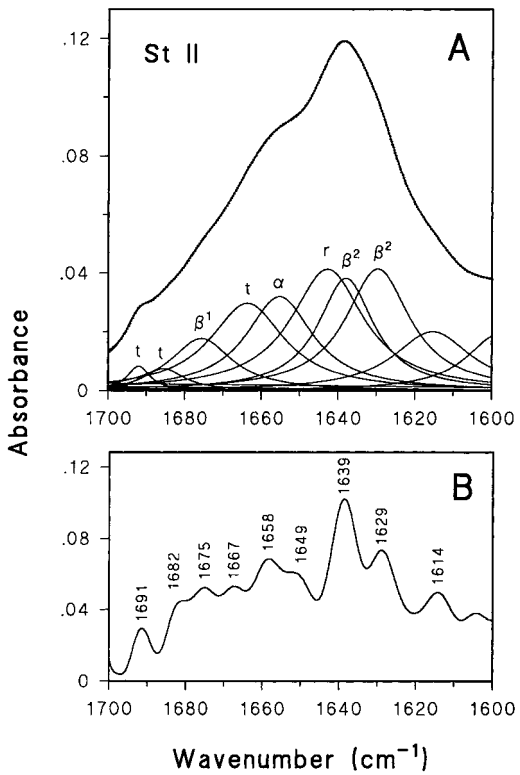

FIG. 1. Infrared-ATR spectra, in the amide I' region, of deuterated films of *S.heliantus* St II. Panel A: The spectrum (solid line), ten Lorentzian component bands obtained by curve-fitting as explained under Methods (thin solid lines) and their sum (dotted line), are shown. Best fitted Lorentzian components were assigned to a particular secondary structure in the usual way (23, 28) and the assignments are indicated next to each band. We used the following criteria: bands in the regions 1696-1680 cm^{-1} and 1670-1660 cm^{-1}, β-turn (t); band at 1675 $\pm$ 4 cm^{-1}, antiparallel β-sheet (β^1 band); band at 1655 $\pm$ 2 cm^{-1}, α-helix (α); band at 1642 $\pm$ 2 cm^{-1}, random coil (r); bands in the region 1640-1620 cm^{-1}, parallel plus antiparallel β-sheet (β^2 bands). The minor bands around 1614 cm^{-1} and 1600 cm^{-1}, were attributed to side chains (29). The evaluated secondary structures are reported in Table 1. Panel B: Deconvoluted spectrum revealing the presence, and approximate position, of the ten components used to fit the original data. We used a resolution enhancement factor 1.6 and Bessel smoothing. The wavenumbers of the major bands observed are indicated.

TABLE 1

FTIR Determination of the Secondary Structure of Sea Anemone Sticholysins

Protein	β^1	β^2	t	α	r	β_{tot} [a]
St I	9	41	19	12	19	69
St I + lipid	7	51	14	18	10	72
St II	8	36	19	15	22	63
St II + lipid	7	49	15	20	9	71

Note. The secondary structure elements were calculated as shown in Fig. 1. Errors of such determinations are typically ±5%. The standard deviations derived from several independent fit were always smaller than this margin.

[a] β_{tot} = β-structure total = $\beta^1 + \beta^2$ + t.

bonding pattern (17, 24, 37), which may occur in very long antiparallel β-strands, as those observed in bacterial porins (34), or in intramolecular bonding ensuing from aggregation. It appears possible that actinoporins open pores by assembling an oligomeric β-barrel through the membrane, like that formed by staphylococcal α-toxin (9). According to a recently proposed hypothesis, this would be consistent also with a symmetrical voltage gating that we have previously observed with St I pores (5), and which seems to be typical for β-barrel channels (38).

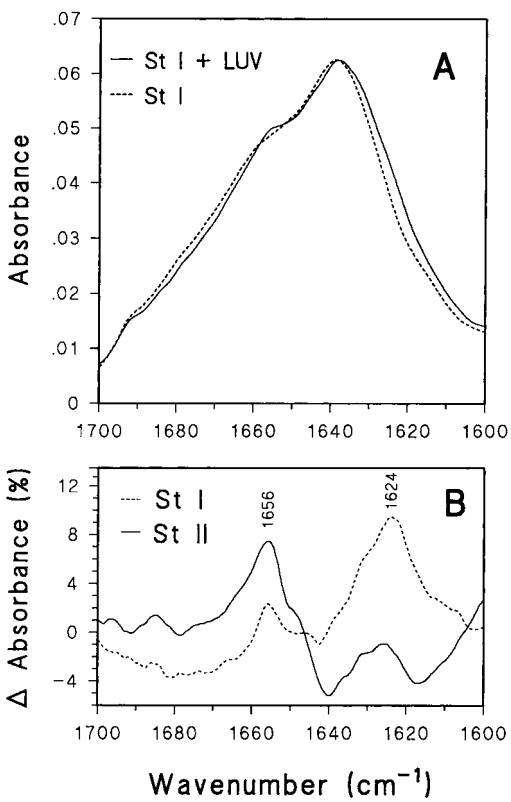

FIG. 2. Infrared-ATR spectra, in the amide I' region, of sticholysins I and II, with and without lipids. The spectrum of St I either in water soluble form (dotted line) or adsorbed to the lipid (solid line), is reported in panel A. The lipid-bound form was normalised in amplitude by multiplying for a constant coefficient (2.3). Differential spectra, obtained by subtracting the soluble form from the normalised lipid-bound form, are shown in panel B, for either St I (dotted line) or St II (solid line). With both cytolysins an excess of signal at 1656 cm^{-1} and 1624 cm^{-1} is present, indicating an increase in α-helix and β-sheet structure (β^2 band), which is paralleled by a deficiency at 1641 cm^{-1}, suggesting a decrease in random coil.

Polarisation experiments and relative orientations of various elements. Spectra collected using linearly polarised light (either at 0° or at 90°) generated several new pieces of information. In first place, from the spectrum polarised at 90°, it was possible to evaluate, via Eq. 4, the lipid to toxin ratio (r) in the LUV/toxin samples. Values of 285 ± 15 and 310 ± 20 were obtained for St I and St II respectively. Compared to the initial value of 250 in the mixture, they indicate that approximately 88 ± 5% of St I and 81 ± 5% of St II bound to the lipid. Consistently, only 10-20% of the initial hemolytic activity was recovered in the supernatant (not shown). From Eq. 5, and using the initial concentrations of lipid and toxin (450 μM and 1.8 μM respectively) we can calculate the partition coefficients. We get 16 ± 5 10^3 M^{-1} and 9 ± 3 10^3 M^{-1} for St I and St II respectively. In the case of St I, this value compares nicely with the experimental value of 13 10^3 M^{-1} that we had previously determined from release experiments (5), under substantially similar conditions.

By analysing the polarised vibrational spectra in the region from 3050 cm^{-1} to 2800 cm^{-1}, corresponding to the stretching of the CH_2 and CH_3 groups (Fig. 3), we could evaluate the average orientation of the lipid chains with respect to the normal to the plane of the crystal (which is the same as the plane of the deposited membranes). After the determination of the dichroic ratio an order parameter was estimated and from this an average angle, as reported in Table 2. The results indicated that the lipid chains formed an angle of about 35° with the normal, a value that is consistent with those published by several authors for phospholipid membranes above the phase transition (18, 33, 39, 40). A similar value was obtained from the dichroic ratio of the amide bond of the ceramide moiety of SM, assuming the C=O stretch is perpendicular to the acyl chain

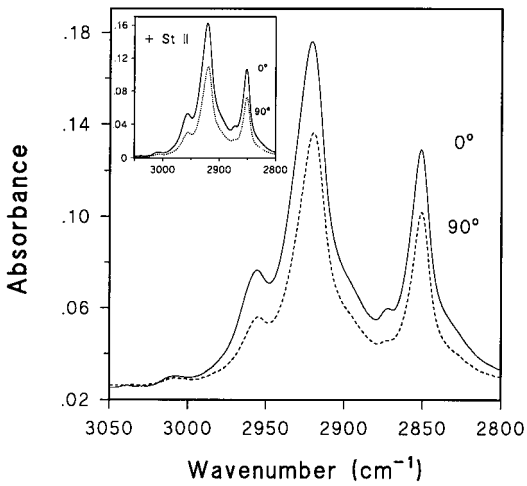

FIG. 3. Infrared-ATR spectra, polarized at 0° and 90°, of depositions of PC:SM LUV, in the region 3050 cm^{-1} to 2800 cm^{-1}. Four absorption bands are evident that correspond to the symmetric and antisymmetric stretching of the CH_2 groups (at 2850 cm^{-1} and 2920 cm^{-1} respectively) and to the symmetric and antisymmetric stretching of the CH_3 groups (at 2872 cm^{-1} and 2956 cm^{-1}). Polarisation parallel to the plane of the reflections in the internal reflecting element (0°) is shown by a solid line, that perpendicular (90°) by a dotted line. The dichroic ratio R was calculated as the ratio of the areas of single Lorentzians fitted to the bands at 0° and 90°. From R, the form factor and the angle relative to the vertical to the plane of the membrane was calculated (see Table 2). In the inset the same spectra, but in the presence of St II adsorbed to the lipids.

direction (40). Upon interaction with the sticholysins, a decrease in order was observed (as with other peptides (33)), leading to an average angle of around 40° with St II and 41° with St I (Table 2).

Finally, the polarisation of the peptide amide I' band was also analysed (Fig. 4). When the ratio of the parallel over the perpendicular spectrum was simply calculated point by point (Fig. 4B), a higher dichroic ratio was found at 1653 cm^{-1}, corresponding to the α-helix component, and at 1627 cm^{-1}, corresponding to the raising β^2 band possibly linked to the formation of an intramolecular β-sheet. Because calculations of average orientations are only possible if the direction of the variation of the dipole moment has a cylindrical distribution around the axis of the structure (e.g. in the case of α-helices and β-barrels), and in the absence of compelling evidences for the formation of a β-barrel in actinoporins, we have limited our analysis to the α-helical component. After curve fitting as above, the contribution of the α-helix band in each spectrum was calculated, and the corresponding dichroic ratio was determined (Table 2). We obtained R = 3.3 with St I and 3.0 with St II. From this, the average angle γ, formed by the molecular axis relatively to the vertical to the plane of the crystal surface, was calculated via Eqs. 1, 2. Values reported by different authors for θ, the mean orientation of the dipole moment around the helix axis, range 22-39° (25, 31, 35). Using an average value of 30° we obtain $\gamma = 38$ with St I and 42° with St II (Table 2). However, if we consider that the lipid chains are also forming an average angle around the vertical direction, and we use Eq. 3 to recalculate the approximate tilting of the alpha-helices with respect to the lipid chains, we obtain an angle of around 13° with St II, and even smaller with St I, which suggest that the helices stay parallel to the lipid chains. These results would be consistent with the hypothesis that, upon binding to the lipid bilayer, the actinoporins insert their amphipathic N-term α-helix through the membrane, thereby stabilising the hydrophilic pores ensuing from aggregation of several monomers (5, 12, 36). However, it is also possible that, albeit oriented perpendicular to the plane of the membrane, the helices are not inserted through it, but rather flank the pore structure at its outside entrance. Finally, we want to mention that we obtained similar results, both in terms

TABLE 2

Assignment and Dichroic Ratio of Some IR Bands Observed in PC/SM Vesicles Alone and with Sticholysins

Wavenumber cm^{-1}	Vibration	Direction[a] θ	Dichroic Ratio	Angle[b] γ	Dichroic Ratio	Angle[b] γ	Dichroic Ratio	Angle[b] γ
			lipid		St I + lipid		St II + lipid	
2920	as CH_2 stretching[c]	90°	1.32 ± .02	35° ± 1°	1.47 ± .03	41° ± 1°	1.45 ± .02	40° ± 1°
2850	s CH_2 stretching	90°	1.33 ± .02	36° ± 1°	1.46 ± .02	40° ± 1°	1.39 ± .04	39° ± 2°
2872	as CH_3 stretching	0°	4.6 ± .2	37° ± 2°	3.5 ± .2	43° ± 1°	3.8 ± .1	40° ± 1°
1590–1680	amid I' SM	90°	1.22 ± .02	32° ± 1°	—	—	—	—
1656	amide I' α-helix	30°	—	—	3.3 ± .1	38° ± 1°	3.0 ± .1	42° ± 1°

Note. Dichroic ratios were obtained as shown in Figs. 3 and 4.

[a] Direction of the variation of the dipole moment associated to the vibration with respect to the direction of the main molecular axis (alifatic chains or α-helix axis).

[b] Average angle between the direction of the molecular axis and the perpendicular to the crystal plane (= membrane plane).

[c] s, symmetric; as, antisymmetric.

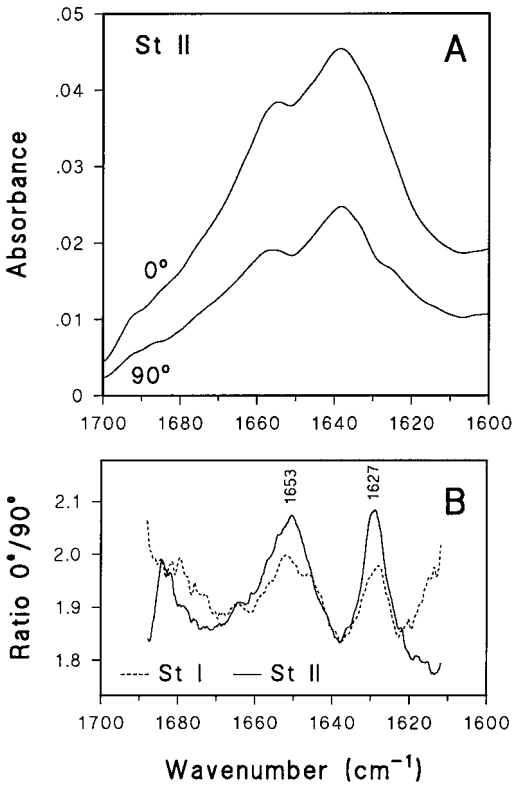

FIG. 4. Infrared-ATR spectra, polarized at 0° and 90°, of sticholysins adsorbed to PC:SM LUV, in the amide I' region. The two spectra for St II, at 0° and 90°, are reported in panel A. The two traces in panel B instead were obtained by ratioing point by point the two spectra (0°/90°) for either St I (dotted line) or St II (solid line). With both cytolysins, the dichroic ratio R was maximum at 1653 cm^{-1} and 1627 cm^{-1}, corresponding to the α-helix and β-sheet structure that increase upon lipid binding, and minimum at 1640 cm^{-1}, which corresponds to the random coil conformation.

of structure and of orientation, also with the parent actinoporin equinatoxin II (not shown).

ACKNOWLEDGMENTS

This work was financially supported by the Italian Consiglio Nazionale delle Ricerche (CNR) and by the Istituto Trentino di Cultura (ITC), with a short term contract to M.T. Equinatoxin II was a kind gift of Professor Peter Macek.

REFERENCES

1. Turk, T. (1991) *J. Toxicol.-Toxin Rev.* **10,** 223–262.
2. Kem, W. R. (1988) *in* The Biology of Nematocysts (Hessinger, D. A., and Lenhoff, H. M., Eds.). pp. 375–405, Academic Press, San Diego.
3. Bernheimer, A. W. (1990) *in* Marine Toxins: Origin, Structure and Molecular Pharmacology (Hall, S., and Strichartz, G., Eds.). pp. 304–311, American Chemical Society, Washington, DC.
4. Macek, P., Belmonte, G., Pederzolli, C., and Menestrina, G. (1994) *Toxicology* **87,** 205–227.
5. Tejuca, M., Dalla Serra, M., Ferreras, M., Lanio, M. E., and Menestrina, G. (1996) *Biochemistry* **35,** 14947–14957.
6. Varanda, A., and Finkelstein, A. (1980) *J. Membr. Biol.* **55,** 203–211.
7. Bernheimer, A. W., and Rudy, B. (1986) *Biochim. Biophys. Acta* **864,** 123–141.
8. Harvey, A. L. (1990) *in* Handbook of Toxinology (Shier, W. T., and Mebs, D., Eds.). pp. 1–66, Marcel Dekker, New York.
9. Song, L., Hobaugh, M. R., Shustak, C., Cheley, S., Bayley, H., and Gouaux, J. E. (1996) *Science* **274,** 1859–1866.
10. Lesieur, C., Vécsey-Semjén, B., Abrami, L., Fivaz, M., and van der Goot, F. G. (1997) *Molec. Membr. Biol.* **14,** 45–64.
11. Pungercar, J., Anderluh, G., Macek, P., Gubensek, F., and Strukelj, B. (1997) *Biochim. Biophys. Acta* **1341,** 105–107.
12. Belmonte, G., Pederzolli, C., Macek, P., and Menestrina, G. (1993) *J. Membr. Biol.* **131,** 11–22.
13. De Los Rios, V., Mancheno, J. M., Lanio, M. E., Onaderra, M., and Gavilanes, J. G. (1998) *Eur. J. Biochem.* **252,** 284–289.
14. Poklar, N., Lah, F., Salobir, M., Macek, P., and Vesnaver, G. (1997) *Biochemistry* **36,** 14345–14352.
15. Anderluh, G., Pungercar, J., Krizaj, I., Strukelj, B., Gubensek, F., and Macek, P. (1997) *Protein Engineering* **10,** 751–755.
16. Macek, P., Zecchini, M., Pederzolli, C., Dalla Serra, M., and Menestrina, G. (1995) *Eur. J. Biochem.* **234,** 329–335.
17. Tamm, L. K., and Tatulian, S. A. (1997) *Q. Rev. Biophys.* **30,** 365–429.
18. Fringeli, U. P., and Günthard, HsH. (1981) *Mol. Biol. Biochem. Biophys.* **31,** 270–332.
19. Blumenthal, K. M., and Kem, W. R. (1983) *J. Biol. Chem.* **258,** 5574–5581.
20. Kem, W. R., and Dunn, B. M. (1988) *Toxicon* **26,** 997–1008.
21. Pederzolli, C., Belmonte, G., Dalla Serra, M., Macek, P., and Menestrina, G. (1995) *Bioconjugate Chem.* **6,** 166–173.
22. MacDonald, R. C., MacDonald, R. I., Menco, B. P. M., Takeshita, K., Subbarao, N. K., and Hu, L. (1991) *Biochim. Biophys. Acta* **1061,** 297–303.
23. Goormaghtigh, E., Cabiaux, V., and Ruysschaert, J.-M. (1990) *Eur. J. Biochem.* **193,** 409–420.
24. Arrondo, J. L., Muga, A., Castresana, J., and Goñi, F. M. (1993) *Prog. Biophys. Molec. Biol.* **59,** 23–56.
25. Menikh, A., Saleh, M. T., Gariepy, J., and Boggs, J. M. (1997) *Biochemistry* **36,** 15865–15872.
26. Arkin, I. T., Rothman, M., Ludlam, C. F. C., Aimoto, S., Engelman, D. M., Rothschild, K. J., and Smith, S. O. (1995) *J. Mol. Biol.* **248,** 824–834.
27. Goormaghtigh, E., Cabiaux, V., and Ruysschaert, J.-M. (1994) *in* Subcellular Biochemistry, Vol. 23: Physicochemical Methods in the Study of Biomembranes, (Hilderston, H. J., and Ralston, G. B., Eds.), pp. 363–403, Plenum Press, New York.
28. Byler, D. M., and Susi, H. (1986) *Biopolymers* **25,** 469–487.
29. Tatulian, S. A., Hinterdorfer, P., Baber, G., and Tamm, L. K. (1995) *EMBO J.* **14,** 5514–5523.
30. Harrick, N. J. (1967) Internal Reflection Spectroscopy, Harrick Scientific Corporation, Ossining, NY.
31. Axelsen, P. H., Kaufman, B. K., McElhaney, R. N., and Lewis, R. N. A. H. (1995) *Biophys. J.* **69,** 2770–2781.
32. Citra, M. J., and Axelsen, P. H. (1996) *Biophys. J.* **71,** 1796–1805.
33. Tamm, L. K., and Tatulian, S. A. (1993) *Biochemistry* **32,** 7720–7726.

34. Rodionova, N. A., Tatulian, S. A., Surrey, T., Jähnig, F., and Tamm, L. K. (1995) *Biochemistry* **34,** 1921–1929.
35. Frey, J., and Tamm, L. K. (1991) *Biophys. J.* **60,** 922–930.
36. Belmonte, G., Menestrina, G., Pederzolli, C., Krizaj, I., Gubensek, F., Turk, T., and Macek, P. (1994) *Biochim. Biophys. Acta* **1192,** 197–204.
37. Goormaghtigh, E., Cabiaux, V., and Ruysschaert, J.-M. (1994) *in* Subcellular Biochemistry, Volume 23: Physicochemical Methods in the Study of Biomembranes, (Hilderston, H. J., and Ralston, G. B., Eds.), pp. 405–450, Plenum Press, New York.
38. Bainbridge, G., Gokce, I., and Lakey, J. H. (1998) *FEBS lett.* **431,** 305–308.
39. Hübner, W., and Mantsch, H. H. (1991) *Biophys. J.* **59,** 1261–1272.
40. Mueller, E., Giehl, A., Schwarzmann, G., Sandhoff, K., and Blume, A. (1996) *Biophys. J.* **71,** 1400–1421.